Fabrication and Properties of Nonreducible Lead-Free Piezoelectric Mn-doped $(Ba,Ca)TiO_3$ Ceramics

Wataru Sakamoto*, Kouta Noritake, Hiroki Ichikawa, Koichiro Hayashi,

Toshinobu Yogo

Division of Materials Research, Institute of Materials and Systems for Sustainability,

Nagoya University, Nagoya 464-8603, Japan

---

* Corresponding author; Tel.: +81 52 7892751; Fax: +81 52 7892133;
E-mail: sakamoto@imass.nagoya-u.ac.jp (W. Sakamoto).

Abstract

Nonreducible lead-free (Ba,Ca)TiO_3 piezoceramics were fabricated by controlling the level of Mn doping. Similar to Mn-doped $(Ba_{0.85}Ca_{0.15})TiO_3$ ceramics sintered in air, stable dielectric properties with temperature change were achieved for the nonreducible sample by stabilizing the tetragonal phase of $BaTiO_3$ over a wide temperature range. In addition, optimization of the level of Mn doping was very effective in improving the sintered density and electrical resistivity for $(Ba_{0.85}Ca_{0.15})TiO_3$ ceramics sintered under a low oxygen partial pressure. The valence state of doped Mn in nonreducible (Ba,Ca)TiO_3 after sintering was confirmed to be Mn^{2+} or Mn^{3+} by electron spin resonance analysis. Sintered bodies of 1 mol% Ba excess and 1 mol% Mn-doped $(Ba_{0.85}Ca_{0.15})TiO_3$, which were sintered at 1350°C in a H_2(0.3%)/Ar atmosphere, exhibited sufficient sintered density and resistivity to allow the characterization of several electrical properties. The ferroelectric, field-induced strain, and piezoelectric properties of the nonreducible $(Ba_{0.85}Ca_{0.15})TiO_3$ ceramics sintered in the reducing atmosphere were comparable with those of $(Ba_{0.85}Ca_{0.15})TiO_3$ samples sintered in air.

Keywords: $BaTiO_3$ and titanates; Dielectric properties; Piezoelectric properties; Mn doping

1. Introduction

Perovskite $Pb(Zr,Ti)O_3$ (PZT)-based ceramics have been widely applied as piezoelectric materials because of their excellent electrical properties [1]. However, toxic PbO is a major component of these materials. Recently, because of growing concerns about the global environment, the development of materials that do not contain toxic elements has been crytical. Therefore, lead-free piezoelectric materials have been extensively studied all over the world [2]. Among several alternatives to PZT, $BaTiO_3$, which exhibits a Curie temperature of $T_C \sim 130°C$ and a high piezoelectric coefficient ($d_{33} \sim$ 190–230 pC/N) [3,4], has been receiving considable attention as a potential candidate. Single-crystal $BaTiO_3$ exhibits a large electric-field-induced strain through control of the engineered domain configuration [5-7]. Furthermore, the phase diagram and characteristic electromechanical response of $(Ba,Ca)TiO_3$ under the application of high electric fields have been examined by several researchers [8-11]. Lead-free piezoelectric $(Ba,Ca)TiO_3$-based materials can partly replace PZT if sufficient properties are achieved.

On the other hand, with progress in the downsizing of piezoelectric actuator devices, multilayer technology is indispensable for achieving high displacement while lowering the working voltage. Because noble metal electrodes are commonly used in current multilayer-type piezoelectric ceramic components, the cost of the internal electrode in this component increases. As for multilayer ceramic capacitors [12], to reduce the cost of the electrodes, the establishment of a co-sintering process with base metal electrodes under a low oxygen partial pressure is required for the production of multilayer

piezoelectric components [13,14]. In this case, nickel is commonly used as an electrode material in such electronic components. In the co-sintering process, the oxygen partial pressure at the sintering temperature should be controlled [for example, below 0.1 Pa (10^{-6} atm) at 1350°C] to suppress the oxidation of nickel metal electrodes. The major problem with $BaTiO_3$-based materials is their low endurance in a reducing atmosphere, which causes a poor insulating resistance (n-type semiconductor characteristics) and makes the evaluation of ferroelectric and piezoelectric properties difficult. The generation of conductive electrons accompanied by the reduction of titanium ions (Ti^{4+}) during the sintering process is the main reason for this problem [12,15,16]. To realize reduction-resistant (= nonreducible) $BaTiO_3$-based ceramics, the effect of Mn, Co, and Mg doping on $BaTiO_3$-based materials was investigated for ceramics sintered in a CO-CO_2 atmosphere [17]. The effects of the A/B ratio in ABO_3 and the substitution of Ca at Ba and Ti sites of $BaTiO_3$ fired in a reducing atmosphere on the improvement of the insulating resistance were also studied [15,16]. The authors have already reported the fabrication and characterization of reduction-resistant grain-oriented $(Ba,Ca)TiO_3$ piezoelectric ceramics [18]. However, the effect of modification of the amount and valence state of dopant ions for $(Ba,Ca)TiO_3$ ceramics remains unclear.

For the purpose of using lead-free $BaTiO_3$ material for multilayer piezoelectric applications at low cost, this paper describes the fabrication and properties of nonreducible $(Ba,Ca)TiO_3$ ceramics to achieve electrical properties comparable to those of samples sintered in air. In particular, the effects of excess Ba composition and the doping level of Mn were examined for reduction-resistant $(Ba_{0.85}Ca_{0.15})TiO_3$ ceramics. The poling condition of the samples was also studied to examine the potential electrical

properties of the resultant Mn-doped $(Ba_{0.85}Ca_{0.15})TiO_3$ ceramics sintered in a reducing atmosphere.

2. Material and methods

2.1 Fabrication of Mn-doped (Ba,Ca)TiO_3 ceramics

The starting materials used for the preparation of the (Ba,Ca)TiO_3 ceramic samples were $BaTiO_3$ (Sakai Chemical, BT-01), $CaTiO_3$ (Kojundo Chemical), $MnCO_3$ (Kojundo Chemical), and $BaCO_3$ (Kojundo Chemical). In the powder compaction method, all the starting materials used to prepare $0.85BaTiO_3$-$0.15CaTiO_3$ with and without 1 mol% $BaCO_3$ and containing various amounts of $MnCO_3$ were weighed and then ball-milled in ethanol for 120 min with a planetary mill (750 rpm) and then cold isostatically pressed at 140 MPa, yielding a green disk compact. Before shaping the green bodies, the powder was treated with a small amount of polyvinyl alcohol (Kishida Chemical) aqueous solution (3 mass%). The green bodies were heat-treated at 500°C for 4 h at a heating rate of 2°C/min in air to remove organic species, followed by heat treatment at 1350°C for 5 h at a rate of 5°C/min in air or an Ar flow containing H_2 (0.3%) atmosphere. Furthermore, $(Ba_{0.85}Ca_{0.15})TiO_3$ sintered pieces were also fabricated using the tape casting method. All starting materials were weighed according to the desired composition as described above and then mixed with a solvent [butyl acetate (Kishida Chemical)], binder [9 mass% with respect to the total oxide powder; polyvinyl butyral (Sekisui Chemical, BL-S)], and plasticizer [7 mass% with respect to the total oxide powder; dibutyl phthalate (Kishida Chemical)]. The mixture was then stirred for 18 h to prepare a slurry of 20 vol% total

inorganic solids. The slurry was tape-cast using an applicator with a gap of 250 μm. After drying, a single-layer sheet was cut, laminated, and hot-pressed at 85°C and pressure of 40 kg/cm^2 for 5 min to form a green compact. The thickness of the compact was approximately 520 μm. The compact was further cut into small pieces of approximately 2 mm width and 2 mm length. The compact was heat-treated at 1350°C for 5 h under the same sintering conditions as the samples from the green disk bodies prepared by the powder compaction method.

2.2 Characterization of Mn-doped (Ba,Ca)TiO_3 ceramics

The crystallographic phases of the sintered bodies were identified by X-ray diffraction (XRD; Rigaku Smart Lab–DPK) analysis using Cu Kα radiation with a monochromator. The microstructures of the samples were examined using scanning electron microscopy (SEM; JEOL, JSM-5600). The valence state of doped Mn in the perovskite (Ba,Ca)TiO_3 crystalline powder prepared by grounding a ceramic body sintered under a low oxygen partial pressure was characterized by electron spin resonance (ESR; JEOL JES-RE1X) spectroscopy at 77 K. To evaluate the electrical properties of the sintered bodies, Ag electrodes were prepared using Ag paste on both sides of the disc-shaped and small-piece specimens, followed by annealing at 650°C for 5 min in air. The dielectric constant was measured at various temperatures with an impedance analyzer (Hioki, IM3570). In addition, polarization (*P*)–electric field (*E*) hysteresis loops were evaluated at room temperature using a virtual ground mode coulomb (*Q*)–voltage (*V*) transducer. A charge amplifier (Kitamoto Electric Co., Ltd., JP001-PE) at 0.1 Hz under electrical fields of 20-40 kV/cm with a high-voltage amplifier

(Trek, 610E) was also used. The field-induced strain coefficient was characterized based on the electric-field-induced displacement of the ceramics using a contact-type displacement meter [19] (Kitamoto Electric Co., Ltd., JP005-2-SE) by dividing the maximum displacement by the maximum applied voltage. A poling treatment was conducted using a direct current (DC) power supply (Trek, 610E) at 20-30 kV/cm in silicon oil at room temperature for 20 min. The resonance frequency at approximately 100 kHz to 1 MHz was measured with an impedance gain phase analyzer (Hioki, IM3570). The planar mode of the electromechanical coupling factor (k_p) and mechanical quality factor (Q_m) were calculated based on the JEITA EM-4501 standard. The small piece samples were used for evaluation of the ferroelectric and electric-field-induced strain properties, and the disk samples were used for the other characterizations.

3. Results and Discussion

3.1 Effect of excess Ba composition in (Ba,Ca)TiO_3 ceramics

Figure 1 shows the XRD patterns of Mn-doped $(Ba_{0.85}Ca_{0.15})TiO_3$ samples prepared in this study. These Mn-doped $(Ba_{0.85}Ca_{0.15})TiO_3$ samples exhibit typical XRD profiles of perovskite tetragonal $BaTiO_3$ phase. Diffraction lines characteristic of similar tetragonal $BaTiO_3$ were also confirmed from the $(Ba_{0.85}Ca_{0.15})TiO_3$ samples without Mn doping. Based on the XRD analysis data, all the fabricated (Ba,Ca)TiO_3 samples in this study were indexed as a perovskite tetragonal $BaTiO_3$ single phase at room temperature.

Excess-barium (*A*-site of ABO_3 compound) has been reported to be effective for improvement of electrical resistivity for $BaTiO_3$-based ceramics sintered in a reducing

atmosphere [16]. In this study, the effect of the barium excess composition (1 mol%) on the microstructure of the resultant ceramics was examined. Figure 2 presents SEM surface images of 0.2 mol% Mn-doped $(Ba_{0.85}Ca_{0.15})TiO_3$ ceramics with and without 1 mol% excess barium sintered in air and a H_2(0.3%)/Ar flow at 1350°C for 5 h. Abnormal grain growth and an inhomogeneous microstructure are observed in the sample (sintered in the air) without excess barium in Fig. 2(a). In this case, the grain size distribution is relatively large, and the grain size ranged from 10 to 70 μm. However, abnormal grain growth was effectively restrained in the sintered bodies in both air (grain size: 2-10 μm) and the reducing atmosphere (grain size: 10-16 μm); for the samples containing excess barium, a relatively homogeneous grain microstructure was also observed (Figs. 2(b) and (c)). Although J.-K. Lee *et al*. reported $BaTiO_3$ ceramics containing 1-3 mol% excess Ba exhibited relatively low sintered densities [20], the current Mn-doped $(Ba_{0.85}Ca_{0.15})TiO_3$ with excess barium was highly densified; the ceramics sintered in both air and the reducing atmosphere exhibited densities around 95%. In the samples with excess barium, pores were hardly observed in the sintered bodies. This result is important for enhancement of the mechanical properties of the samples as a polycrystalline piezoelectric and for reproducibility of the experimental data. The grain size of the sample prepared in the reducing atmosphere increased slightly because defects might be easily formed in the crystal grain and grain boundary, and diffusion of constituent elements was promoted at high temperatures.

3.2 Sintered density and dielectric properties of nonreducible Mn-doped $(Ba,Ca)TiO_3$ ceramics

In this study, calcium was selected for substitution at the Ba sites of $BaTiO_3$. The ionic radius of Ca^{2+} is smaller than that of Ba^{2+}, and Ca^{2+} is reported to have partially off-center positions in the perovskite oxide lattice [9,10]. Such off-center positions of Ca^{2+} have been reported to induce an effective dipole, which may enhance the ferroelectricity and piezoelectricity of the solid solution [21]. The ratio of Ba to Ca and the barium excess composition in $(Ba,Ca)TiO_3$ were fixed at 0.85/0.15 and 1 mol%, respectively. A previous study [16] showed that at this composition, the degradation of insulating resistance can be suppressed for $(Ba,Ca)TiO_3$ ceramics sintered even in a reducing atmosphere. Therefore, (considering the data shown in Figs. 1 and 2,) evaluation from here on was conducted for the samples of Mn-doped $(Ba_{0.85}Ca_{0.15})TiO_3$ with 1 mol% excess Ba composition.

Figure 3 shows the temperature dependences of the dielectric constant of the 0.2 mol% Mn-doped $(Ba_{0.85}Ca_{0.15})TiO_3$ ceramics with 1 mol% excess Ba composition sintered in air and a H_2 (0.3%)/Ar flow at 1350°C for 5 h. Both ceramic samples exhibited sufficient electrical resistivity (higher than 10^{10} Ω·cm) for this measurement. Their microstructures are also shown in Figs. 2(b) and (c). For the reducing atmosphere condition in this study, the nickel metal powder compact heat-treated under the same conditions was confirmed to be not oxidized. Therefore, the oxygen partial pressure was below 0.1 Pa (10^{-6} atm) at 1350°C. In addition, the oxygen partial pressure at 1350°C in the furnace was measured to range from 10^{-9} to 10^{-11} atm using a zirconia oxygen sensor. The change in the dielectric constant with temperature was measured for the unpoled sample at 1 kHz. The measurement data adopts the value in the heating process. When measuring at each temperature, time was spent to sufficiently stabilize the sample

temperature. Although the peak top slightly shifted, both the $(Ba_{0.85}Ca_{0.15})TiO_3$ ceramic samples exhibited phase transition behavior similar to that of reported $(Ba_{0.9}Ca_{0.1})TiO_3$ ceramics sintered in air [22]. These samples exhibited only one peak, corresponding to a phase transition in their ε_r–T curve. In addition, the properties were affected by several additive elements in this study, and the Curie temperature shifted to the low-temperature side. In the temperature range in Fig. 3, pure $BaTiO_3$ exhibited two peaks at approximately 0°C and 130°C [9]. The former peak corresponds to the transition from the orthorhombic to the tetragonal phase, and the latter peak corresponds to the transition from the tetragonal to the cubic phase. In particular, it has been reported that the former temperature might shift toward the lower-temperature region when Ca is substituted at Ba sites, enlarging the tetragonal phase area [8,9]. This behavior was also observed in the reduction-resistant $(Ba_{0.85}Ca_{0.15})TiO_3$ ceramic.

In this study, the effect of the Mn doping level on the sintered density and electrical resistivity of the $(Ba_{0.85}Ca_{0.15})TiO_3$ ceramic samples (with 1 mol% excess Ba composition) sintered at a low oxygen partial pressure was also investigated. Figure 4 shows the electrical resistivity and relative density of the $(Ba_{0.85}Ca_{0.15})TiO_3$ ceramics sintered in a reducing atmosphere at 1350°C for 5 h as a function of Mn concentration. Fig. 4(a) shows that sufficient electrical resistivity was achieved for the samples sintered in a reducing atmosphere. When the amount of doped Mn was more than approximately 1 mol%, the electrical resistivity increased. This finding is the characteristic effect of Mn acceptor ions according to the following formulas:

$$2MnO \rightarrow 2Mn_{Ti}^{''} + 2O_O + 2V_O^{\bullet\bullet} \qquad \cdots \quad (1)$$

$$Mn_2O_3 \rightarrow 2Mn_{Ti}^{'} + 3O_O + V_O^{\bullet\bullet} \qquad \cdots \quad (2)$$

In formulas (1) and (2), when the Mn ion having a lower valence state than the Ti ion is replaced with the Ti site, oxygen vacancies are formed in the crystal lattice. Because of this, the equilibrium is considered to shift toward the side where the generation of oxygen vacancies during firing in the reducing atmosphere is suppressed by increasing the oxygen vacancy concentration according to the Mn doping (in these cases, Mn^{2+} and Mn^{3+}). In addition, the sintered density was highest when the amount of Mn doping was 1 mol%, as observed in Fig. 4(b). Based on the results, 1 mol% Mn-doped $(Ba_{0.85}Ca_{0.15})TiO_3$ with 1 mol% excess Ba composition was selected as a standard composition for reduction-resistant $(Ba_{0.85}Ca_{0.15})TiO_3$ in this study.

3.3 Valence state analysis of nonreducible Mn-doped (Ba,Ca)TiO_3 ceramics

To predict the valence state of Mn in the $(Ba_{0.85}Ca_{0.15})TiO_3$ ceramics sintered in a reducing atmosphere, ESR measurements were performed for the grounded powder of the perovskite 1 mol% Mn-doped $(Ba_{0.85}Ca_{0.15})TiO_3$ ceramic (with 1 mol% excess Ba composition) to obtain the characteristic spectrum. Figure 5 presents the ESR spectrum of the 1 mol% Mn-doped $(Ba_{0.85}Ca_{0.15})TiO_3$ powder at 77 K (frequency of microwave: 9.3 GHz). The valence state of Mn in the sample was evaluated based on the *g*-factor and hyperfine structure of the nuclear spin ($I = 5/2$) of Mn. This powder exhibited a hyperfine structure with characteristic six-line splitting (*g* value: 2.000) resulting from the spin $I = 5/2$ of the Mn nucleus. The hyperfine constant estimated from the division width of the signal was 8.8 mT. This signal was demonstrated to originate from typical Mn^{2+} by comparing it with the spectrum of a Mn^{2+}-diffused MgO standard sample. Mn^{2+} in the $(Ba_{0.85}Ca_{0.15})TiO_3$ ceramics is considered to be partially oxidized to higher valent cations,

and Mn^{2+} and Mn^{3+} occupy the Ti^{4+} site with a mixed valent state because Mn^{3+} cannot be detected by ESR measurements. The existence of Mn^{3+} here needs to be confirmed by other analysis methods such as X-ray photoelectron spectroscopy, etc. in the future. The signal from Mn^{4+} was not observed in the Mn-doped $(Ba_{0.85}Ca_{0.15})TiO_3$ sample in this study. A similar signal of Mn^{2+} of perovskite ABO_3 oxides has been reported in $PbTiO_3$ [23], $(K_{0.5}Na_{0.5})NbO_3$ [24], and $(Bi_{0.5}Na_{0.5})TiO_3$ [25]. The reduction-resistant Mn-doped $(Ba_{0.85}Ca_{0.15})TiO_3$ ceramics (Mn > 0.8 mol%) prepared in this study exhibited sufficient insulating resistance (> 10^{11} Ω·cm). The high insulating properties of the ceramics sintered in the reducing atmosphere are attributed to capturing of the conduction electrons generated in the $(Ba_{0.85}Ca_{0.15})TiO_3$ by its valence change of Mn (in this case, between Mn^{2+} and Mn^{3+}), as described in the following formula:

$$Mn'_{Ti} + e^- \rightarrow Mn''_{Ti} \ (Mn^{3+} \rightarrow Mn^{2+}) \quad \cdots(3)$$

In the present case, doped Mn (1 mol%) is considered to be substituted at the Ti^{4+} sites in $(Ba_{0.85}Ca_{0.15})TiO_3$ and to behave as an acceptor, leading to the reduction-resistant nature as discussed in a previous report [12].

3.4 Ferroelectric and field-induced strain properties of Mn-doped (Ba,Ca)TiO_3 ceramics

Figure 6 presents the *P–E* hysteresis loops and unipolar electric field-induced strain curves of Mn-doped $(Ba_{0.85}Ca_{0.15})TiO_3$ ceramics with 1 mol% excess Ba composition. Figs. 6(a)-(c) present data for the sample sintered in air without Mn doping,

the 0.2 mol% Mn-doped sample sintered in air, and the 1.0 mol% Mn-doped sample sintered in a H_2(0.3%)/Ar atmosphere at 1350°C for 5 h, respectively. The samples exhibited sufficient insulating resistance for high electric fields to be applied to evaluate their ferroelectric and piezoelectric properties. These data were measured at room temperature and a frequency of 0.1 Hz. All the samples exhibited characteristic *P–E* and field-induced strain loops of ferroelectrics. In particular, both Mn-doped $(Ba_{0.85}Ca_{0.15})TiO_3$ ceramics in Fig. 6(a) exhibited a well-shaped ferroelectric *P–E* hysteresis loop with a remanent polarization (P_r) of 7.0-7.5 μC/cm^2 and coercive field (E_c) of 4.5-5.5 kV/cm. Furthermore, from the unipolar field-induced strain curves [Fig. 6(b)], the strain at 40 kV/cm and field-induced strain constant, which was calculated from the slope of the loop, of the nonreducible Mn-doped $(Ba_{0.85}Ca_{0.15})TiO_3$ were also determined to be comparable to that of the ceramic sintered in air. The maximum strain and estimated field-induced strain constant of the nonreducible Mn-doped $(Ba_{0.85}Ca_{0.15})TiO_3$ attained values of approximately 0.13% and 260 pm/V, whereas those of the Mn-doped $(Ba_{0.85}Ca_{0.15})TiO_3$ ceramic sintered in air were 0.14% and 270 pm/V, respectively. With Mn doping, the ferroelectric and field-induced strain properties of the $(Ba_{0.85}Ca_{0.15})TiO_3$ ceramics were improved as observed in Fig. 6. The dopant Mn effectively suppresses the degradation of insulating resistance at high applied voltages. Furthermore, by optimizing the Mn doping level, similar properties were obtained for both samples sintered in air and a reducing atmosphere.

3.5 Piezoelectric properties of Mn-doped (Ba,Ca)TiO_3 ceramics after poling treatment

Figure 7 presents typical data on the frequency dependences of the phase and impedance of the nonreducible 1 mol% Mn-doped $(Ba_{0.85}Ca_{0.15})TiO_3$ ceramics (with 1 mol% excess Ba composition) prepared in this study. This sample exhibits a distinctive resonance-antiresonance signal. The poling treatment of the sample was performed under the poling condition of 30 kV/cm and at room temperature for 20 min. The phase (θ_{max}) of the poled sample reached approximately 86° as observed in Fig. 7, which indicates that the poling treatment was successfully performed. However, the phase of the previously reported nonreducible 1 mol% Mn-doped $(Ba_{0.85}Ca_{0.15})TiO_3$ randomly-oriented ceramic was 83^o, which indicates that the degree of poling treatment (20 kV/cm at room temperature for 20 min) was not sufficiently achieved for piezoelectric characterization [18].

Table 1 summarizes several properties of the Mn-doped $(Ba_{0.85}Ca_{0.15})TiO_3$ ceramics with 1 mol% excess Ba composition sintered in air and the reducing atmosphere. These measurements were performed at room temperature. The dielectric constants of the samples after the poling treatment were approximately 1100 at 1 kHz. The dielectric loss was also comparable (approximately 0.009). Therefore, their dielectric properties did not change significantly. The value of $-d_{31}$ for the sample sintered under a low oxygen partial pressure in Table 1 is comparable that of the $(Ba_{0.85}Ca_{0.15})TiO_3$ sample sintered in air. The k_p and Q_m values of the $(Ba_{0.85}Ca_{0.15})TiO_3$ sample sintered in the reducing atmosphere were higher than those of the sample sintered in air. In this case, the amount of Mn doping of the nonreducible $(Ba,Ca)TiO_3$ sample was larger than that of the ceramic sintered in air. The main reason for the higher Q_m is related to the formation of defects of the reduction-resistant sample, as described in formulas (1) and (2), because

Q_m is correlated to the amount of oxygen vacancies in $BaTiO_3$-based ceramics. The nonreducible samples became more hard piezoelectric compared with the samples sintered in air. The piezoelectric properties depend not only on the amount of oxygen vacancies but also on the degree of poling. The phase (θ_{max}) of the poled sample sintered in air was approximately 76°. Furthermore, the $(Ba_{0.85}Ca_{0.15})TiO_3$ ceramics with 0.2 mol% of Mn sintered in the reducing atmosphere had insufficient electrical insulation properties and the θ_{max} value also had a relatively low value (below 40°) after the poling treatment, so it is difficult to compare piezoelectric characteristics, and various piezoelectric data are not listed in Table 1. In the future, examining the domain structure of samples sintered in both air and a reducing atmosphere is important. Standard PZT at the morphotropic phase boundary is reported to have an electromechanical coupling factor (k_p) above 0.5 and a mechanical quality factor (Q_m) of approximately 500 [26]. In addition, for the enhancement of the piezoelectric properties, forming a solid solution with other perovskite oxides ($BaZrO_3$ and $BaSnO_3$, etc.) to modify the ferroelectric domain structure, and controlling the crystal growth orientation are critical. These approaches are currently being investigated.

4. Conclusions

Reduction-resistant $(Ba,Ca)TiO_3$ ceramics with high sintered density, homogeneous grain microstructure and improved electrical resistivity were fabricated by modifying the chemical composition with the excess Ba and Mn doping. The tetragonal phase of $BaTiO_3$ was stabilized over a wide temperature range by the formation of a solid solution

with $CaTiO_3$ even in the nonreducible $(Ba,Ca)TiO_3$ samples. Furthermore, Mn doping was very effective in improving the ferroelectric and field-induced strain properties for $(Ba_{0.85}Ca_{0.15})TiO_3$ ceramics sintered in both air and an Ar flow containing H_2 (0.3%). ESR analysis revealed that doped Mn existed as Mn^{2+} or Mn^{3+} in $(Ba_{0.85}Ca_{0.15})TiO_3$ ceramics sintered under a low oxygen partial pressure of below 0.1 Pa (10^{-6} atm). Mn ions might work as acceptors for capturing conductive electrons with its valence change. The ferroelectric and field-induced strain properties of the 1 mol% Mn-doped $(Ba_{0.85}Ca_{0.15})TiO_3$ ceramics sintered in the reducing atmosphere were comparable to those of the 0.2 mol% Mn-doped $(Ba_{0.85}Ca_{0.15})TiO_3$ sintered in air. By performing appropriate poling treatment, the poling state of the nonreducible $(Ba_{0.85}Ca_{0.15})TiO_3$ ceramics was improved, leading to the observation of potential piezoelectric properties. Although further enhancements of the piezoelectric properties are still required, the reduction-resistant $(Ba,Ca)TiO_3$-based ceramics in this study are expected to be promising candidates for lead-free ceramic materials for multilayer piezoelectric component applications.

Acknowledgement

This work is partly supported by the Hosokawa Powder Technology Foundation.

References

[1] G.H. Haertling, Ferroelectric ceramics: History and technology, J. Am. Ceram. Soc. 82 (1999) 797-818.

[2] T.R. Shrout, S.J. Zhang, Lead-free piezoelectric ceramics: Alternatives for PZT?, J. Electroceram. 19 (2007) 113-126.

[3] R. Bechman, Elastic, Piezoelectric, and dielectric constants of polarized barium titanate ceramics and some applications of the piezoelectric equations, J. Acoust. Soc. Am. 28 (1956) 347-350.

[4] D. Berlincourt, H.H.A. Krueger, Dependence of the ratio of piezoelectric coefficients on density and composition of barium titanate ceramics, Phys. Rev. 105 (1957) 56-57.

[5] P.W. Rehrig, S.E. Park, S. Trolier-McKinstry, G.L. Messing, B. Jones, T.R. Shrout, Piezoelectric properties of zirconium-doped barium titanate single crystals grown by templated grain growth, J. Appl. Phys. 86 (1999) 1657-1661.

[6] S. Wada, S. Suzuki, T. Noma, T. Suzuki, M. Osada, M. Kakihana, S.-E. Park, L.E. Cross, T.R. Shrout, Enhanced piezoelectric property of barium titanate single crystals with engineered domain configurations, Jpn. J. Appl. Phys. 38 (1999) 5505-5511.

[7] Z. Yu, R. Guo, A.S. Bhalla, Dielectric polarization and strain behavior of $Ba(Ti_{0.92}Zr_{0.08})O_3$ single crystals, Mater. Lett. 57 (2002) 349-354.

[8] T. Mitsui, W.B. Westphal, Dielectric and X-ray studies of $Ca_xBa_{1-x}TiO_3$ and $Ca_xSr_{1-x}TiO_3$, Phys. Rev. 124 (1961) 1354-1370.

[9] D. Fu, M. Itoh, S. Koshihara, T. Kosugi, S. Tsuneyuki, Anomalous phase diagram of ferroelectric $(Ba,Ca)TiO_3$ single crystals with giant electromechanical response, Phys. Rev. Lett. 100 (2008) 227601.

[10] D. Fu, M. Itoh, S. Koshihara, Crystal growth and piezoelectricity of $BaTiO_3$–$CaTiO_3$ solid solution, Appl. Phys. Lett. 93 (2008) 012904.

[11] D. Fu, M. Itoh, S. Koshihara, Invariant lattice strain and polarization in $BaTiO_3$–$CaTiO_3$ ferroelectric alloys, J. Phys.: Condens. Matter 22 (2010) 052204.

[12] H. Kishi, Y. Mizuno, H. Chazono, Base-metal electrode-multilayer ceramic capacitors: Past, present and future perspectives, Jpn. J. Appl. Phys. 42 (2003) 1-15.

[13] S. Kawada, M. Kimura, Y. Higuchi, H. Takagi, (K,Na)NbO_3-based multilayer piezoelectric ceramics with nickel inner electrodes, Appl. Phys. Express 2 (2009) 111401.

[14] H. Hayashi, S. Kawada, M. Kimura, Y. Nakai, T. Tabata, K. Shiratsuyu, K. Nada, H. Takagi, Reliability of nickel inner electrode lead-free multilayer piezoelectric ceramics, Jpn. J. Appl. Phys. 51 (2012) 09LD01.

[15] Y. Sakabe, Dielectric materials for base-metal multilayer ceramic capacitors, Am. Ceram. Soc. Bull. 66 (1987) 1338-1341.

[16] Y. Sakabe H. Takagi, Nonreducible mechanism of $\{(Ba_{1-x}Ca_x)O\}_mTiO_2$ (m>1) ceramics, Jpn. J. Appl. Phys. 41 (2002) 6461-6465.

[17] I. Burn, G.H. Maher, High resistivity $BaTiO_3$ ceramics sintered in CO-CO_2 atmosphere, J. Mater. Sci. 10 (1975) 633-640.

[18] H. Ichikawa, W. Sakamoto, Y. Akiyama, H. Maiwa, M. Moriya T. Yogo, Fabrication and characterization of (100),(001)-oriented reduction-resistant lead-free piezoelectric (Ba,Ca)TiO_3 ceramics using platelike seed crystals, Jpn. J. Appl. Phys. 52 (2013) 09KD08.

[19] Y. Akiyama, T. Hayashi, Electric-field-induced strain in lead lanthanum zirconate titanate ceramics, Jpn. J. Appl. Phys. 37 (1998) 5297-5300.

[20] J.K. Lee, K.S. Hong, Roles of Ba/Ti ratios in the dielectric properties of $BaTiO_3$ ceramics, J. Am. Ceram. Soc. 84 (2001) 2001–2006.

[21] J.G. Bednorz, K.A. Müller, $Sr_{1-x}Ca_xTiO_3$: An XY quantum ferroelectric with transition to randomness, Phys. Rev. Lett. 52 (1984) 2289-2292.

[22] D. Tanaka, J. Yamazaki, M. Furukawa, T. Tsukada, High power characteristics of $(Ca,Ba)TiO_3$ piezoelectric ceramics with high mechanical quality factor, Jpn. J. Appl. Phys. 49 (2010) 09MD03.

[23] K. Hayashi, A. Ando, Y. Hamaji Y. Sakabe, Study of the valence state of the manganese ions in $PbTiO_3$ ceramics by means of ESR, Jpn. J. Appl. Phys. 37 (1998) 5237-5240.

[24] Y. Kizaki, Y. Noguchi, M. Miyayama, Defect control for low leakage current in $K_{0.5}Na_{0.5}NbO_3$ single crystals, Appl. Phys. Lett. 89 (2006) 142910.

[25] W. Sakamoto, N. Makino, T. Katayama, M. Moriya, T. Yogo, Improvement of the ferroelectric properties of chemically synthesized $Bi_{1/2}Na_{1/2}TiO_3$ thin films via Mn doping, Ferroelectrics 479 (2015) 56-63.

[26] B. Jaffe, W.R. Cook, H. Jaffe, Piezoelectric Ceramics, Academic Press, New York, 1971, pp. 135-160.

List of Table

List of Figures

1.0 mol% (BCT15-1.0Mn) sintered in H_2(0.3%)/Ar atmosphere at 1350°C for 5 h (measured at room temperature; frequency, 0.1 Hz).

Fig. 7, Frequency dependences of impedance and phase of 1 mol% Mn-doped $(Ba_{0.85}Ca_{0.15})TiO_3$ ceramics (with 1 mol% excess Ba composition) sintered at 1350°C for 5 h in H_2(0.3%)/Ar atmosphere (measured at room temperature).

Table 1, Properties of Mn-doped $(Ba_{0.85}Ca_{0.15})TiO_3$ ceramics with 1 mol% excess Ba composition sintered at 1350°C for 5 h (measured at room temperature).

Sintering atmosphere	Relative density (%)	$\varepsilon_{33}^T/\varepsilon_0$ [1 kHz]	Electrical resistivity ($10^{10}\,\Omega\cdot$cm)	$-d_{31}$ (pC/N)	k_p (%)	Q_m
Air *[1]	99	1040	31.8	38	27	250
H_2(0.3%)/Ar *[2]	99	1130	12.6	39	31	640

*[1]: 0.2 mol% Mn, *[2]: 1.0 mol% Mn doping

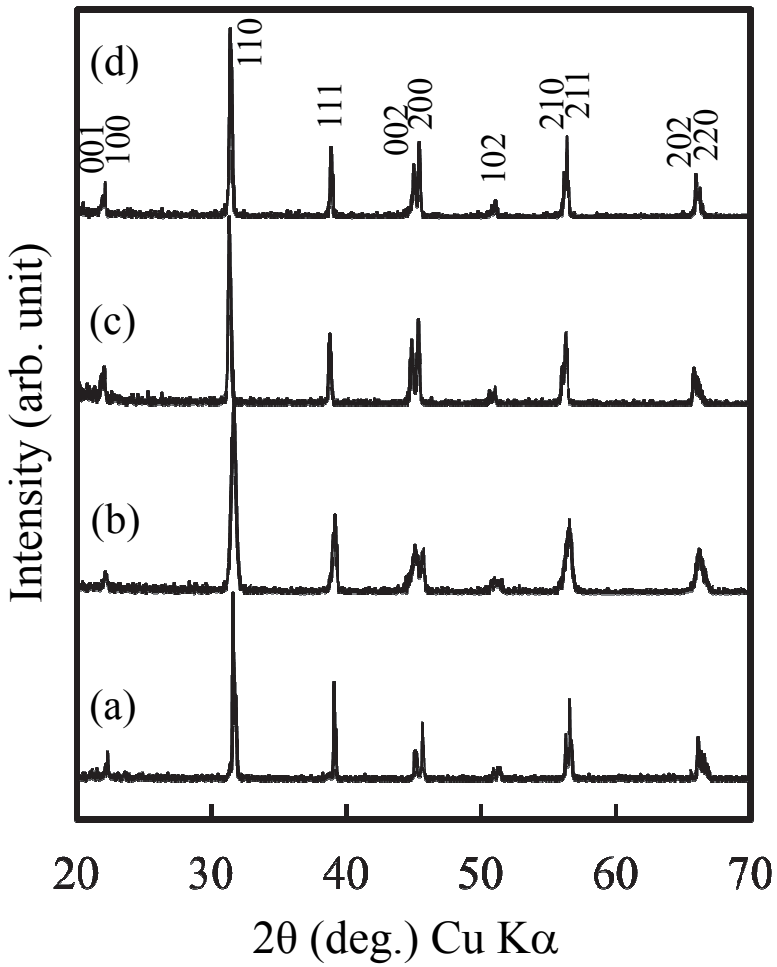

Fig. 1, XRD patterns of 0.2 mol% Mn-doped $(Ba_{0.85}Ca_{0.15})TiO_3$ ceramics [(a) without and (b) with 1 mol% excess Ba composition] sintered in air, and Mn-doped $(Ba_{0.85}Ca_{0.15})TiO_3$ ceramics with 1 mol% excess Ba and [(c) 0.2 mol% Mn and (d) 1 mol% Mn] in a H_2(0.3%)/Ar flow. [Sintering condition: 1350°C, 5 h]

Fig. 1 Sakamoto *et al*.

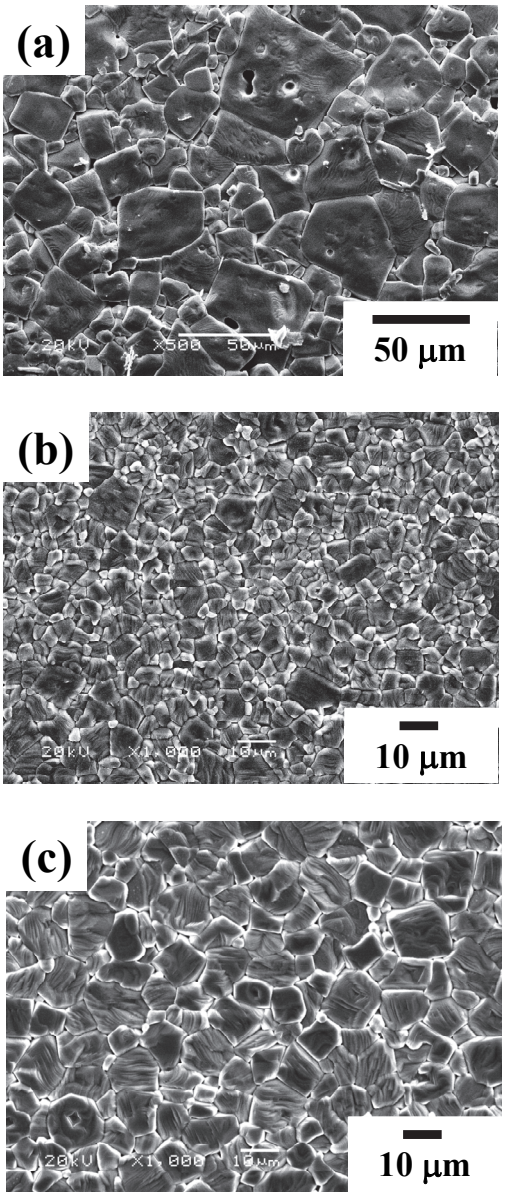

Fig. 2, SEM surface images of 0.2 mol% Mn-doped $(Ba_{0.85}Ca_{0.15})TiO_3$ ceramics (a) without and (b), (c) with 1 mol% excess Ba composition [sintered in (a), (b) air and (c) a H_2(0.3%)/Ar flow at 1350°C for 5 h].

Fig. 2 Sakamoto *et al*.

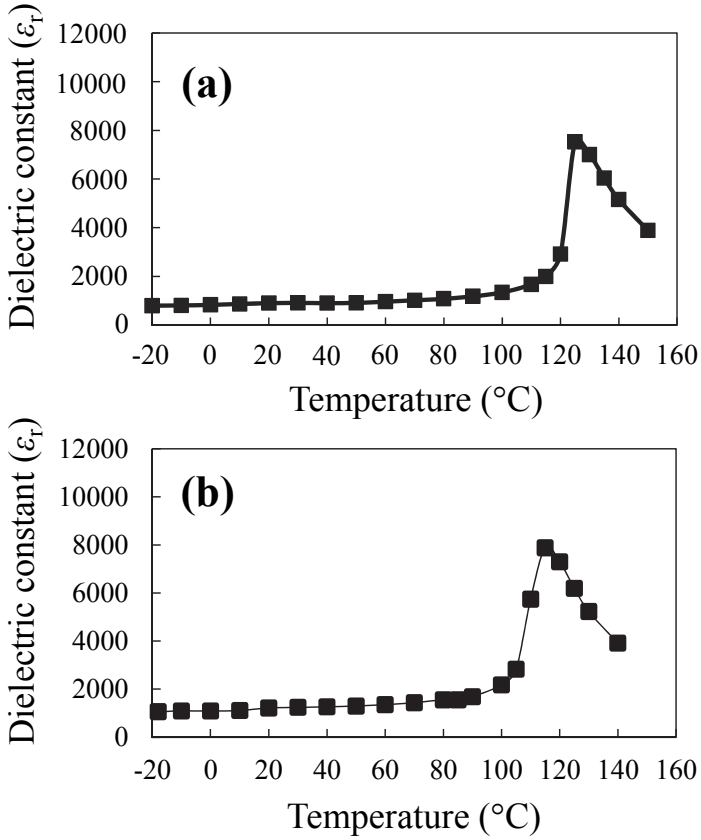

Fig. 3, Temperature dependence of dielectric constant for unpoled 0.2 mol% Mn-doped $(Ba_{0.85}Ca_{0.15})TiO_3$ ceramics (with 1 mol% excess Ba composition) sintered in (a) air and (b) a H_2(0.3%)/Ar flow at 1350°C for 5 h.

Fig. 3 Sakamoto *et al*.

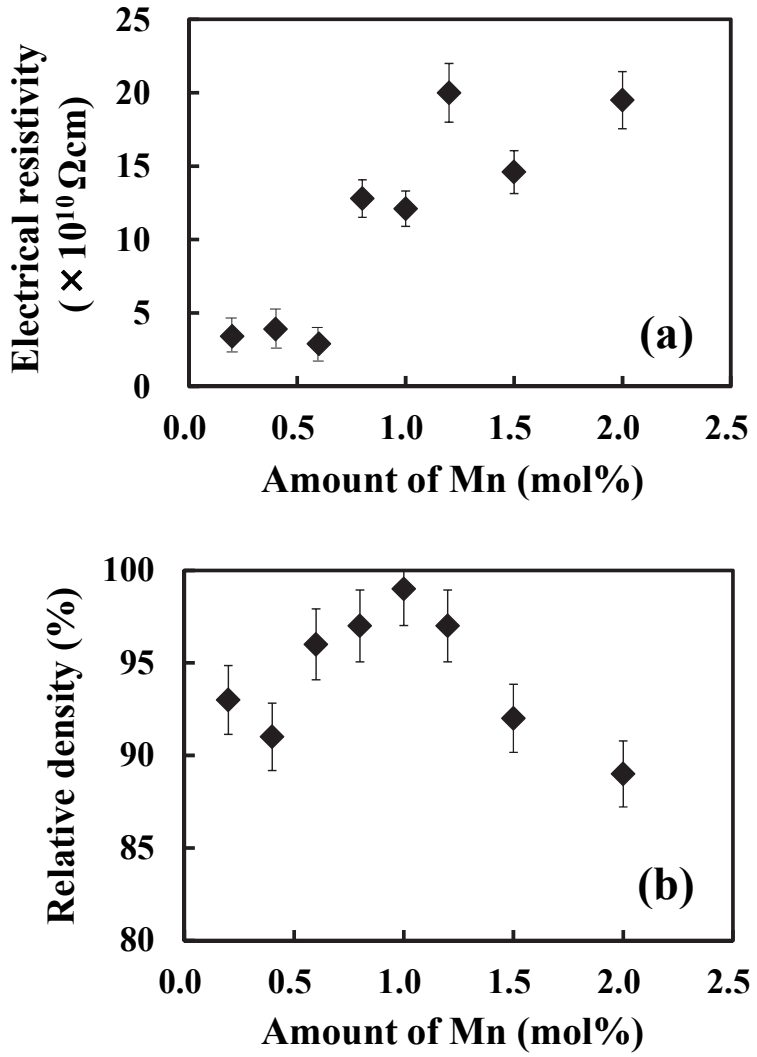

Fig. 4, (a) Electrical resistivity and (b) relative density of Mn-doped $(Ba_{0.85}Ca_{0.15})TiO_3$ ceramics (with 1 mol% excess Ba composition) sintered in reducing atmosphere at 1350°C for 5 h as a function of Mn concentration.

Fig. 4 Sakamoto *et al*.

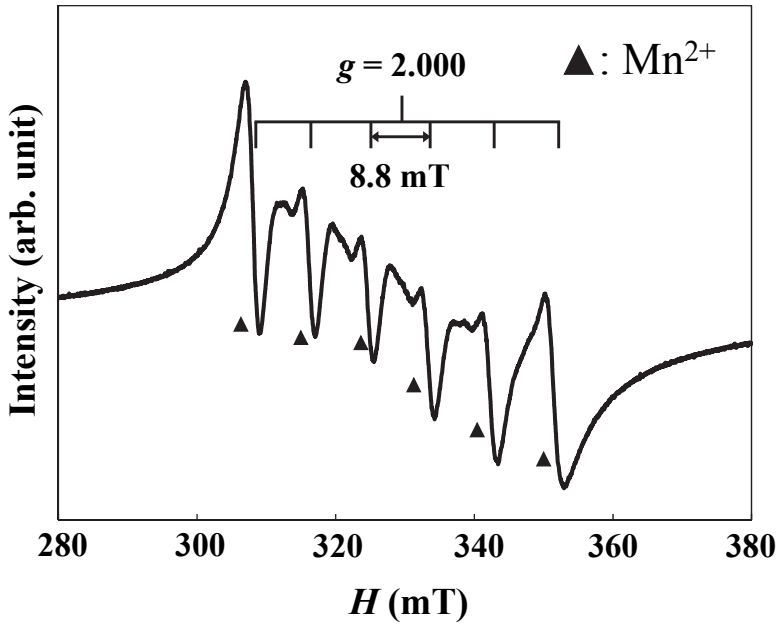

Fig. 5, ESR spectrum of 1 mol% Mn-doped $(Ba_{0.85}Ca_{0.15})TiO_3$ powder (with 1 mol% excess Ba composition) after grinding of sintered body (measured at 77 K).

Fig. 5 Sakamoto *et al*.

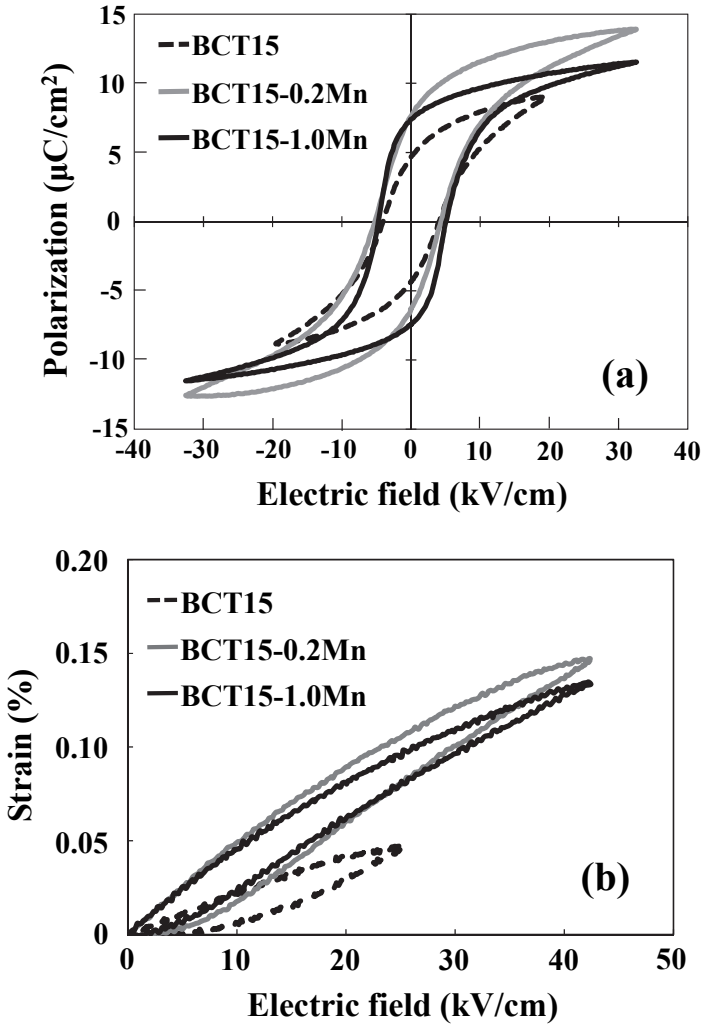

Fig. 6, *P–E* hysteresis loops and unipolar electric field-induced strain curves of $(Ba_{0.85}Ca_{0.15})TiO_3$ ceramics with 1 mol% excess Ba composition and Mn doping: (a) 0 mol% (BCT15) sintered in air, (b) 0.2 mol % (BCT15-0.2Mn) sintered in air, and (c) 1.0 mol% (BCT15-1.0Mn) sintered in H_2(0.3%)/Ar atmosphere at 1350°C for 5 h (measured at room temperature; frequency, 0.1 Hz).

Fig. 6 Sakamoto *et al*.

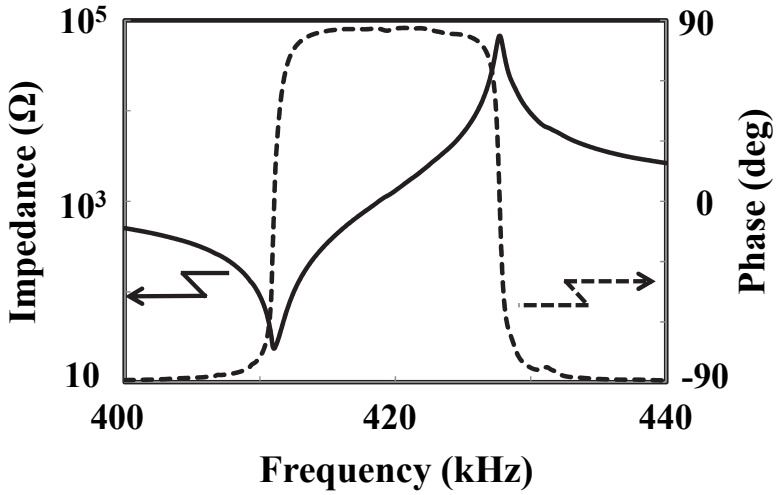

Fig. 7, Frequency dependences of impedance and phase of 1 mol% Mn-doped $(Ba_{0.85}Ca_{0.15})TiO_3$ ceramics (with 1 mol% excess Ba composition) sintered at 1350°C for 5 h in H_2(0.3%)/Ar atmosphere (measured at room temperature).

Fig. 7 Sakamoto *et al*.